Probing acetylated-α-synuclein monomer–aggregate complexes by NMR elucidates mechanism of fibril seeding

Xue Yang[1], Baifan Wang[1], Cody L. Hoop[1], Jonathan K. Williams[1], and Jean Baum[1*]

[1]Department of Chemistry and Chemical Biology, Rutgers University, Piscataway, New Jersey 08854

*Corresponding author: Jean Baum; Dept. of Chemistry and Chemical Biology, Rutgers University, 123 Bevier Rd., Piscataway, NJ 08854; Tel.: 848-445-5284; Email: jean.baum@chem.rutgers.edu

Classification
Biological Sciences (Major), Biophysics and Computational Biology (Minor)

Keywords
Amyloid formation, Amyloid seeding, IDP–IDR interactions, Aggregation inhibition, Parkinson's Disease

Author Contributions

X.Y., B.W., and J.B. designed research; X.Y., B.W., and C.L.H. performed research; X.Y., B.W., C.L.H., J.K.W., and J.B. analyzed data; and X.Y., B.W., C.L.H., J.K.W., and J.B. wrote the paper.

This PDF file includes:

Main Text
Figures 1–7

Abstract
Amyloid fibril formation of α-synuclein (αS) is associated with multiple neurodegenerative diseases, including Parkinson's Disease (PD). Growing evidence suggests that progression of PD is linked to cell-to-cell propagation of αS fibrils, which leads to templated seeding of endogenous intrinsically disordered monomer. A molecular understanding of the seeding mechanism and driving interactions is crucial to inhibit progression of amyloid formation. Here, using relaxation-based solution NMR experiments designed to probe large complexes, we identify weak interactions of intrinsically disordered acetylated-αS (Ac-αS) monomers with seeding-competent Ac-αS fibrils and seeding-incompetent off-pathway oligomers to elucidate amyloid promoting interactions at the atomic level. We identify a binding interface in the first 11 residues of the N-terminus that interacts with both fibrils and off-pathway oligomers, under conditions that favor fibril elongation. This common N-terminal hotspot is supported by suppression of seeded amyloid formation by oligomers, as observed through thioflavin-T fluorescence experiments, suggesting competing monomer interactions. This highlights that an amyloid-incompetent species of αS itself can act as an auto-inhibitor against αS fibril elongation. The similarity between the fibril and oligomer structures lies in their intrinsically disordered termini. Thus, we propose that the monomer–aggregate interactions occur between the intrinsically disordered monomer N-terminus and the intrinsically disordered regions (IDRs) of the fibril/oligomers. Taken together, we propose a novel Ac-αS seeding mechanism that is driven by the recruitment of intrinsically disordered monomers by the fibril IDRs, highlighting the potential of the terminal IDRs of the fibril rather than the structured core, as new therapeutic targets against seeded amyloid formation.

Significance
Cell-to-cell spreading of α-synuclein (αS) fibrils leads to amyloid seeding of endogenous monomer. A detailed atomic-level mechanistic understanding of the fibril seeding process of αS is essential for design of therapeutic approaches against Parkinson's disease. In light of its complexity, this process remains ill-defined at the molecular level. Using relaxation-based solution NMR experiments, we are able to map the binding interface of the acetylated αS (Ac-αS) intrinsically disordered monomer with seeding-competent Ac-αS fibrils and seeding-incompetent off-pathway oligomers to elucidate the critical monomer–aggregate seeding interactions in early and late stages of aggregation. From this work, we propose a new paradigm, in which the αS seeding process is initiated by monomer recruitment through the intrinsically disordered N- and C-termini on the fibril surface, which may provide novel therapeutic targets against amyloid formation.

1. Introduction

Amyloid formation of the intrinsically disordered protein (IDP) α-Synuclein (αS) is closely associated with the pathogenesis of a variety of neurodegenerative disorders, including Parkinson's disease (PD), dementia with Lewy bodies, and multiple-systems atrophy (1). The pathology of αS is still not clearly understood, as multiple species along the fibril aggregation pathway, including on-pathway oligomeric intermediates and end-stage fibrils, have been demonstrated to be toxic to neurons (2-8). Abrogation of these toxic species is extremely challenging, in part due to perpetual fibril fragmentation and seeding once amyloidogenesis commences. The amyloid seeding process is a complex mechanism by which monomers interact with existing fibril seeds to facilitate additional fibril formation. This mechanism involves multiple microscopic steps, including elongation of fibril ends and surface-mediated secondary nucleation (9-11). Furthermore, disease progression has become increasingly linked to prion-like cell-to-cell propagation of αS aggregates, in which αS oligomers and fibrils are transmitted to neighboring neurons (12, 13). Here, the invading aggregates seed amyloid formation of endogenous monomers to accelerate production of toxic species (3). Thus, disruption of the process by which αS aggregates seed proliferative amyloid formation has become an intriguing target for inhibition of pathological αS self-assembly and may reveal new therapeutic approaches against PD.

Under amyloid fibril formation conditions in vitro, αS monomers self-assemble along multiple pathways to mature into various species of oligomers in parallel with fibrils (Figure 1a). This includes multiple oligomeric species that do ("on-pathway") or do not ("off-pathway") convert into amyloid fibrils. While the inherent structural inhomogeneity and transient nature of on-pathway oligomers makes them extremely challenging to isolate and characterize, off-pathway oligomers are stable and can be isolated by size exclusion chromatography (SEC) (17). These stable oligomers have been previously found to be composed of monomers oriented in an ellipsoid shape, with the outer layer being made up of flexible and disordered molecules (17) (Fig. 1a). During amyloid formation, monomers, oligomers, and fibrils co-exist together and interact with each other. Distinguishing features of how monomers interact with fibril-seeding or non-seeding aggregates may unveil molecular determinants of fibril propagation and provide insight into pathological seeding processes.

Structural models derived from solid-state nuclear magnetic resonance (NMR) and cryo-electron microscopy (EM) have revealed that αS fibrils consist of two protofilaments with a rigid "Greek key" core flanked by intrinsically disordered N- and C-termini (~40 residues each) (18-22) (Figure 1a). These intrinsically disordered regions (IDRs) are a substantial fraction of the fibril structure and make up a "fuzzy coat" that surrounds the rigid core (18-20). It has been observed previously that the rigid core can act as a template to seed fibril formation (23, 24), yet the role of the IDRs in fibril seeding is not at all understood. Recent studies have shown that pathologically relevant N- and C-terminal truncations modulate the aggregation and seeding propensity of αS fibrils and influence resulting fibril morphologies (25-27). This suggests that the terminal IDRs are also actively involved in the αS aggregation mechanism. In order to more effectively inhibit fibril-seeded propagation, it is critical to identify the initial monomer–fibril interactions, whether they involve the rigid core or the flanking IDRs.

Previous approaches to inhibit different aspects of amyloid fibril seeding have largely targeted the structured amyloid core. Such methods include using chaperones to block fibril ends or fibril surfaces (9), treating with natural products that promote fibril clustering to reduce fibril fragmentation and hide binding sites for monomer addition (14, 15), and creating high affinity interactions with amyloidogenic monomers to sequester monomers from self-assembly (16). However, all of these approaches introduce foreign molecules and can only interfere with single microscopic steps. Thus, they do not provide efficient means to inhibit the auto-catalytic seeding/aggregation processes.

In order to elucidate the molecular determinants of fibril seeding, we use solution NMR spectroscopy to directly probe acetylated-αS (Ac-αS) monomer interactions with seeding-competent Ac-αS fibrils and seeding-incompetent off-pathway Ac-αS oligomers. Off-pathway oligomers that are formed in parallel with amyloid fibrils, but do not themselves convert to amyloid fibrils (Figure 1a), are viable candidates for a non-seeding control. Through relaxation-based NMR experiments under conditions of templated elongation, we find that fibrils and off-pathway oligomers are in a dynamic equilibrium with monomers, and that monomers interact with fibrils and off-pathway oligomers via an intrinsically disordered N-terminal hotspot. We observe by thioflavin T (ThT) fluorescence that off-pathway oligomers act as auto-inhibitors of amyloid formation when co-existing with monomers and fibrils. This may be explained by competing monomer interactions between fibrils and off-pathway oligomers through their common binding modes, whereby the off-pathway oligomers can sequester monomers to reduce monomer interactions with growing fibrils, slowing amyloid formation. The common Ac-αS monomer N-terminal hotspot for seeding-competent fibrils and seeding-incompetent off-pathway oligomers leads us to hypothesize that the terminal IDRs of the aggregates, a shared feature of these structures, play a critical role in the amyloid seeding mechanism. While the structured fibril core is known to be critical to the templated assembly of amyloid fibrils, it is imperative to consider the role of the N and C-terminal fibril IDRs in seeding and fibril assembly and their potential as targets against amyloid propagation.

2. Results

Establishing off-pathway oligomers as a seeding-incompetent control.

Two species of stable αS oligomers were isolated by size-exclusion chromatography (SEC) (Figure S1a) that do not convert to fibrils and do not seed amyloid formation of αS monomers (Figure 1b). These oligomers were prepared from N-terminally acetylated-αS monomers under fibril formation conditions, at 37°C with 300 rpm shaking for 5 h. All αS used in these studies is N-terminally acetylated, since the N-terminus of αS is post-translationally acetylated in vivo (2). N-terminal acetylation increases the helical propensity of the N-terminus, enhances membrane binding (28, 29), and has been shown to influence fibril formation kinetics and morphologies of fibrils produced (30). Thus, interactions of N-terminally acetylated-αS (Ac-αS) monomers with seeding-competent and seeding-incompetent aggregates is physiologically significant to understand seeding mechanisms.

Both species of stable Ac-αS oligomers show a similar distribution of secondary structures by circular dichroism, with reduced β-sheet content relative to mature fibrils (Figure S1b). However, they are distinct from each other in size and morphology. “Big oligomers” show an

overall elongated, worm-like morphology as visualized by transmission electron microscopy (TEM) (Figure 1c), while small oligomers are uniformly circular in shape (Figure S1e). Both big and small oligomers are similar in size and morphology to non-acetylated αS oligomer species previously isolated (17). Although they are formed under fibril formation conditions, these oligomers are considered "off-pathway" since in isolation they do not progress to amyloid fibrils upon incubation at 37°C for 5 days, as evidenced by the lack of ThT fluorescence enhancement (Figure S1c). Moreover, the oligomers maintain their respective morphologies without evidence of fibril formation after 42 days of incubation at 37°C as assessed by TEM (Figure S1f,g). Neither big nor small oligomers can seed amyloid fibril formation when co-incubated with Ac-αS monomer at 37°C within 5 days, as detected by ThT fluorescence (Figure 1b). In addition, these stable oligomers are not converted to fibrils by incubation with pre-formed Ac-αS fibril seeds over five days, as detected by ThT (Figure S1d). Taken together, these results establish these isolated big and small oligomers as off-pathway species that can be used as negative controls of seeding.

Fibrils and off-pathway oligomers are in a dynamic equilibrium with monomers.
Seeding-competent fibrils and seeding-incompetent off-pathway oligomers were characterized by NMR. Fibrils were sonicated prior to seeding, which reduces the heterogeneity of fibril lengths (Fig. S2a, d–f) and increases the number of fibril ends to promote elongation (31) (Fig. S2b). A ^{1}H–^{15}N HSQC spectrum of the sonicated fibril seeds, whose morphology and length distribution were identified by TEM (Figure S3a) is shown in Figure 2a. Because these species are large and tumble slowly in solution, their NMR spectra are expected to contain very few cross-peaks, corresponding to residues primarily from the intrinsically disordered N- and C-terminal domains. Indeed, the ^{1}H–^{15}N HSQC spectrum of the sonicated fibril shows a narrow range of ^{1}H chemical shifts, characteristic of IDPs. The fibril, which would display distinct chemical shifts corresponding to β-sheet secondary structure primarily from the NAC domain, is not observed. Direct comparison of the ^{1}H–^{15}N HSQC spectrum of the sonicated fibril with a spectrum of the Ac-αS monomer under the same conditions, shows that the chemical shifts in the fibril sample and monomer sample are in fact identical (Figure 2a). This suggests that the signals observed in the spectrum of sonicated fibrils in solution arise uniquely from a population of dissociated monomers, and that these monomers are in equilibrium with the fibril.

Similarly, SEC and NMR experiments indicate that both big and small oligomers in solution are also in equilibrium with monomers. After being isolated by SEC, oligomers were immediately re-injected onto the SEC column, and a monomer peak re-emerged (Figure S3b). This indicates that oligomers are continuously in equilibrium with monomer, and monomers cannot be completely separated from the system. These oligomers also show chemical shifts indicative of the intrinsically disordered Ac-αS monomer in their ^{1}H–^{15}N HSQC spectra (Figure S4d,e). However, the peak intensity of C-terminal residues are slightly increased relative to the N-terminal and NAC residues (Figure S5a,b), suggesting that residues in the C-terminal domain of both monomeric and oligomeric species are detected. This is consistent with other αS oligomers that were speculated to maintain mobility in residues 86 and onward based on solution NMR spectra (32). Preferential detection of a disordered C-terminal domain in oligomeric species indicates that they probably make up the "fuzzy" surface of the oligomer (Figure 1a, 3f).

Identification of an Ac-αS N-terminal hotspot for fibril and oligomer interactions.

NMR relaxation experiments were performed to assess residue-specific perturbation of backbone dynamics in sonicated fibril or off-pathway oligomer samples. The detected monomers in equilibrium with sonicated fibrils show substantially elevated ^{15}N-transverse relaxation rates (R_2) in the N-terminal region (first 23 residues), especially in the early N-terminus (residues 2–11) (Figure 2b). An increase in ^{15}N-R_2 is indicative of reduced backbone motions on the picosecond–nanosecond timescale, which may be due to site-specific direct interactions or slowing of global molecular tumbling, or to enhanced conformational exchange on the microsecond–millisecond timescale. The contribution of conformational exchange was assessed by ^{15}N in-phase Hahn echo experiments (Figure 2d), which estimate the exchange contribution to the observed ^{15}N-R_2 as ^{15}N-R_{ex}. No significant R_{ex} is observed in either the monomer or sonicated fibril sample.

Similarly to the fibrils, Ac-αS oligomer samples have increased ^{15}N-R_2 relative to monomers alone in the N-terminus (first 22 residues) with additional increased ^{15}N-R_2 in the late NAC and C-terminus (Figure 2c, S5c). Based on the increased peak intensity in the C-terminus of the oligomer samples and previous proposals that the C-terminus is disordered in αS oligomers (32), the observed increase of ^{15}N-R_2 in the late NAC and C-terminus is likely due to superposition of oligomer and monomer signals. Since both oligomers and monomers in solution provide NMR signal intensity for residues in the C-terminus, the contribution to the apparent ^{15}N-R_2 from these two species cannot be deconvoluted. We expect that the intrinsically disordered segments of the oligomer would be detectable but exhibit slower molecular tumbling as part of the oligomeric complex than that of monomer free in solution. This would result in a globally increased ^{15}N-R_2 of the intrinsically disordered segments of the oligomer relative to that of the monomer. However, the N-terminus of the oligomer is expected to be rigid, buried within the oligomeric core (17, 32) and thus undetectable by solution NMR. The elevated apparent ^{15}N-R_2 in the N-terminus of the oligomer sample instead indicates perturbation of monomer N-terminal backbone dynamics when in equilibrium with these oligomers. This may be explained by monomer N-terminal interactions with the oligomers at the same residues identified to be perturbed in the fibril sample.

In order to determine if the enhanced ^{15}N-R_2 of the monomer in equilibrium with the sonicated fibrils is due to direct contacts, we used ^{15}N-dark state exchange saturation transfer (DEST) (33, 34) experiments. These experiments indirectly probe the NMR-invisible, high molecular weight, "dark" state (fibril-bound Ac-αS monomer) by monitoring residue-specific perturbations in peak intensities in the NMR-visible "light" state (free Ac-αS monomer), through transfer of off-resonance saturation from fibrils to monomers. ^{15}N-DEST experiments were performed on ^{15}N-Ac-αS monomer in the absence of fibrils, and ^{15}N-Ac-αS sonicated fibrils in equilibrium with monomers. Residue-specific peak intensity loss in the equilibrium monomer spectra at multiple distant ^{15}N-offsets relative to isolated monomer is indicative of residues in exchange with the fibril-bound state. This is observed as an effective broadening of the DEST saturation profile in the presence of fibrils. We find that the broadening of the DEST saturation profiles in the presence relative to in the absence of fibrils ($\Delta\Theta$) is localized primarily to the early N-terminus (first 12 residues) (Figure 3a). Representative DEST saturation profiles acquired with 350 Hz RF saturation for residues in each of the three domains in isolated Ac-αS monomer or equilibrium Ac-αS monomer are provided in Figures 3b-e. For residues D2 and V3 in the N-terminus, a clear broadening of the profile is observed in the case of the monomer in equilibrium with fibril relative to the isolated monomer (Figure 3b–c). However, for residues T64 in the NAC and N103

in the C-terminus, minimal differences are observed between the two samples (Figures 3d–e). A simple two-state model that accounts for one NMR-visible state (free monomer) and one NMR-invisible state (monomer bound to fibril) fits to residue-specific ΔR_2 values (R_2^{fibril}-$R_2^{monomer}$) and DEST profiles with 350 Hz and 150 Hz RF saturation (Figure S5, Fig. 3b–e). Based on this model, 99.79 ± 0.05% of the monomer is in the free state while the remainder is bound to the fibril with an apparent first order rate constant (k_{on}^{app}) of 2.36 ± 0.08 s^{-1}. Despite this low population of fibril-bound monomer, substantially higher R_2^{bound} values, on the order of 10^3–10^5 s^{-1} (Figure S6), are estimated for the first 11 residues relative to the remainder of the sequence. These two analyses of the ^{15}N-DEST data, calculation of $\Delta\Theta$ and simulated estimations of R_2^{bound} values, suggest that under the condition where there is a large population of mature fibrils, a low population of monomers in equilibrium with the fibrils directly interact with the fibrils via an N-terminal hotspot that includes the first 11 residues. N-terminal residues that exhibit increased ^{15}N-R_2 values but do not show the DEST effect are likely not in direct contact with the aggregates, but may still be impacted by the interaction due to their proximity to the binding site. Together, these data suggest that both sonicated fibrils and off-pathway oligomers are in dynamic equilibrium with dissociating Ac-αS monomers and that the monomer–fibril direct contacts involve the early monomer N-terminus, which is potentially also an interaction domain for off-pathway oligomers (Figure 3f).

N-terminal hotspot is conserved at early-stage aggregation.

The results in the previous section describe how pre-formed fibrils and oligomers, species that are dominant in the late stages of aggregation, are associating and dissociating with monomeric Ac-αS. But what initial monomer interactions with fibril seeds or seeding-incompetent oligomers occur to influence seeded amyloid formation at the early stages of aggregation, when the concentration of monomeric Ac-αS is much larger than any aggregates? Solution NMR spectroscopy was again utilized to directly probe the site-specific interactions of Ac-αS monomers with fibrils or off-pathway oligomers. Under conditions of excess monomeric Ac-αS, no chemical shift perturbations are observed in the ^{1}H–^{15}N HSQC spectra of Ac-αS monomers upon addition of any of the aggregates (Figure S4a–c). This is consistent with the lack of chemical shift perturbations observed in the ^{1}H–^{15}N HSQC spectra of fibril and oligomer samples described above (Figure 2a, S4d,e), confirming that monomeric Ac-αS is observed under both conditions. Interestingly, upon addition of either fibrils or off-pathway oligomers, changes are observed in the monomer dynamics, with the strongest increases in ^{15}N-R_2 observed in the first 9 residues of the N-terminus (Figure 4a and b), consistent with the late-stage results above. Monomer residues in direct contact with fibrils were probed through ^{15}N-DEST experiments. The low, although apparent, DEST effect in the excess monomer case combined with the low signal intensities at these monomer concentrations, results in high errors in the calculated $\Delta\Theta$ of the DEST profiles (Figure 4c). Despite this, a greater DEST effect is observed for the first 11 residues by this analysis. Although the ΔR_2s of monomer in the presence versus in the absence of fibrils is low (< 0.9 s^{-1}), residue-specific ΔR_2 values and DEST profiles were fit to a two-state model. Based on this model, less than 0.2% of the monomer is bound to the fibril seeds in solution with an estimated k_{on}^{app} of 0.8 s^{-1}. Despite the low population of fibril-bound monomer and slow unbound–bound interconversion rate, the per-residue R_2^{bound} calculations show especially high values (10^4–10^5 s^{-1}) for the first 9 N-terminal residues (Figure S7). This is consistent with analysis of broadening of the DEST profiles, and points to the same binding site determined for monomers with late-stage fibrils. Together, ^{15}N-R_2 perturbation and ^{15}N-DEST

results indicate that the monomer N-terminus is the primary interaction site for both fibrils and off-pathway oligomers, under conditions of both early-stage and late-stage seeded aggregation. Sequence analysis of the N-terminal domain shows that this region is highly conserved (Figure 4d), further suggesting that the αS N-terminal domain is a hotspot for functional interactions.

Competitive Ac-αS monomer–fibril and monomer–oligomer interactions delay fibril elongation.

Aggregation of Ac-αS from the initial monomer form results in a dynamic mixture of fibrils and off-pathway oligomers that are present simultaneously in solution. The amyloid indicating ThT fluorescence change was used to investigate the interplay of off-pathway oligomers co-existing with Ac-αS monomers and fibrils during aggregation. Ac-αS monomer was seeded with 1 μM Ac-αS pre-formed fibrils under conditions that promote elongation (10 mM PBS, pH 7.4), rather than secondary nucleation, with varying concentrations of either big or small oligomers under quiescent conditions at 37°C and monitored by ThT fluorescence to probe the time-dependent formation of fibrils. A significant delay in fibril formation is observed upon addition of 2x molar excess of big oligomers to fibril seeds, and by adding big oligomers at a 5x molar excess to fibril seeds amyloid formation is essentially abolished, as evidenced by the almost complete loss of ThT fluorescence intensity (Figure 5a). A similar inhibitory effect is also observed for the small oligomers (Figure S8c), indicating that fibril formation is significantly delayed in the presence of off-pathway oligomers. After five days of co-incubation with big or small oligomers, fibrils show morphology that is indistinguishable from the initial fibril seeds, which suggests that the oligomers modify and significantly delay the kinetics of seeded fibril formation, but do not change the morphology of the mature fibrils produced (Figure S8d–f).

The inhibitory effect of the off-pathway oligomers is reduced by promoting elongation, either by sonication of pre-formed fibril seeds or by increasing concentration of monomers. Sonication of fibril seeds reduces the fibril length from micrometers to nanometers and produces more fibril ends, which provide more elongation sites for the same monomer-equivalent seed concentration (Figure S2a,b) (10, 31, 35). Consistent with the literature, the longer the sonication time applied to mature fibrils, the shorter the fibril seeds, the more numerous the elongation-competent ends, and the more efficient the seeding capacity (Figure S2a,b,d–f). Using fibrils (1 μM monomer equivalent) that have been sonicated for extended periods of time as seeds, and co-incubating them with oligomers (2 μM monomer equivalent) and 40 μM monomers, the oligomer inhibitory effect on the aggregation kinetics is largely reduced (Figure 5b, S8a). Likewise, under the same conditions, increasing the monomer concentration corresponds to faster aggregation kinetics (Figure S2c). With increasing monomer concentration, we observe shorter lag times even in the presence of oligomers (Figure 5c, S8b). Thus under conditions promoting fibril elongation, enhanced monomer–fibril interactions from increasing fibril ends or increasing monomer concentration reduces the inhibitory effect of off-pathway oligomers.

Taken together, our results suggest that off-pathway oligomers formed in parallel with amyloid fibrils suppress fibril elongation through competitive interactions with Ac-αS monomers via a conserved 11-residue N-terminal hotspot. Since off-pathway oligomers and fibrils interact with the same N-terminal residues of the Ac-αS monomers, the availability of monomers to interact with fibrils is reduced, effectively inhibiting amyloid fibril propagation.

Off-pathway Ac-αS oligomers are non-toxic to SH-SY5Y cells.
Extensive work has been done to investigate the observed toxicity of αS fibrils, and while an exact understanding of the mechanism has not been reached, αS amyloid fibrils are thought to exert their toxic effect through interactions with multiple different cellular pathways (18, 36-38). Oligomers have also shown significant levels of cellular toxicity (8, 39, 40). MTS (3-(4,5-dimethylthiazol-2-yl)-5-(3-carboxymethoxyphenyl)-2-(4-sulfophenyl)-2H-tetrazolium) cell viability assays were used to evaluate the potential toxicity of the big and small oligomers used in this work. After incubating SH-SY5Y neuronal cells with Ac-αS fibrils for 24 h, cell viability is reduced in a dose dependent manner (Figure 6a, gray). However, when treating SH-SY5Y cells with the either big or small off-pathway oligomers (up to 5 μM monomer equivalent) for 24 h, no significant MTS reduction is observed (Figure 6a, red, blue). To ensure an accurate assessment of fibril or oligomer entry into the cells, SH-SY5Y cells were treated with fibrils or off-pathway oligomers covalently linked with ATTO-488. After 24 h incubation, cells were stained with DAPI and purified mouse anti-αS antibody (Figure 6b,c). Cells treated with either fibrils or off-pathway oligomers showed cellular entry of the aggregates (Figure 6c, green). Fibril treated cells show 3.3 fold higher anti-αS fluorescence relative to monomer control cells, indicating that fibrils or other aggregates efficiently accumulate in the cellular environment. However, cells treated with big or small oligomers only show 1.34 fold and 1.76 fold higher anti-αS fluorescence relative to monomer treated cells, respectively. Thus, these off-pathway oligomers do not induce significant accumulation of αS aggregates in the cellular environment.

3. Discussion

Fibril seeding is an important process in the propagation and cell-to-cell spreading of disease related amyloid fibrils. Understanding the monomer interactions that initiate fibril seeding in the early stages, and that promote amyloid growth in the late stages of aggregation, is critical for effective interference with aggregation processes. In the case of the Parkinson's related Ac-αS, we observe that Ac-αS fibril and oligomer species are dynamic entities existing in equilibrium with monomeric Ac-αS. This is consistent with previous NMR translational diffusion results that indicated a population of monomer-like species in solution with Ac-αS fibrils (41), and with the concept of molecular recycling of amyloid fibrils first introduced with fibrils of the SH3 domain (42). However, residue-specific ^{15}N-R_2s of these equilibrium monomers relative to free monomers suggest that they are not completely "free", but rather specifically re-associate with the fibrils and oligomers. Through ^{15}N-DEST experiments, the first 11 N-terminal residues of Ac-αS monomers were found to be the binding domain for fibrils in late-stages of aggregation. This same N-terminal region shows enhanced ^{15}N-R_2 values in monomers in equilibrium with off-pathway oligomers, suggesting a similar monomer binding mode. In addition, we find that analogous interactions occur in a seeding environment when monomer is in excess of seeding-competent fibrils or seeding-incompetent oligomers. NMR relaxation and ^{15}N-DEST experiments indicate a localized N-terminal interaction hotspot in the first 9–11 residues in the presence of off-pathway oligomers or fibril seeds. This suggests that fibril seeding is an equilibrium process: adding excessive monomer will promote fibril formation, while continuously removing monomer promotes fibril disaggregation. This idea has been confirmed by fluorescence work, which shows that αS fibrils will disaggregate when the protein concentration is lower than a critical concentration (43).

The environment becomes more complex, however, as amyloid aggregation proceeds through multiple parallel pathways that result in disordered aggregates, stable oligomers, or amyloid fibrils (44). This raises the importance of understanding the interactions between the multiple co-existing species of the same protein along parallel aggregation pathways. Here we show that the stable off-pathway Ac-αS oligomers formed under fibril-promoting conditions are not merely bystanders in the aggregation process, but delay seeded monomer amyloid formation kinetics. By probing monomer–off-pathway oligomer and monomer–fibril residue-specific interactions, we find that both off-pathway oligomers and fibrils weakly interact with the first 11 residues of the monomer N-terminus. The N-terminus of αS has been recognized as an interaction hotspot that may contribute to induction or inhibition of amyloid formation. N-terminal interactions of αS monomers with chaperones (45) and nanoparticles (46) have been shown to inhibit amyloid formation, and recently a canonical motif for transient interactions of αS with chaperones was determined (45), which shares the 11 N-terminal amino acids identified here. In this work, the shared monomer binding site for off-pathway oligomers and fibrils suggests that the oligomers can delay fibril formation through competitive interactions with monomers. Through monomer interactions with off-pathway oligomers, the concentration of monomers available for propagating fibrils is reduced, effectively delaying amyloid formation. Inhibition of fibril growth by co-existing species has been proposed for other amyloid-forming proteins, such as insulin, lysozyme, and Aβ (47, 48).

The identification of a conserved N-terminal hotspot on Ac-αS monomers for interaction with both off-pathway oligomers and fibrils suggests a common interaction mechanism. The remarkable similarity in the monomer recognition site is at first surprising, given the vast difference in morphologies between off-pathway oligomers and fibrils. However, similarity between the fibril and oligomer structures lies in their intrinsically disordered termini. Oligomers purified under amyloid-forming conditions were determined to have a fuzzy outer shell made up by the disordered C-termini using small-angle X-ray scattering (17, 49) (Figure 3f). This "fuzzy-coat" is observed by NMR through increased signal intensity in the C-terminal residues, both in this work's off-pathway oligomer samples (Figure 2c, S5a,b) and in αS oligomers reported by others (32). With this "fuzzy-coat" model, only the C-terminus of αS in the oligomer is exposed for interactions with monomers (Figure 7). The N-terminal interaction hotspot on the monomer contains several lysine residues, which may be attracted to the highly negatively charged C-terminus of the oligomer. Conversely, αS amyloid fibrils possess both exposed disordered N- and C-termini flanking a rigid Greek-key fibril core, as observed in structural models determined by solid-state NMR and cryo-electron microscopy (18-22). In this way, αS fibrils also have a "fuzzy-coat" made of disordered C-termini (~residues 97-140) in addition to a "fuzzy-coat" made of disordered N-termini (~residues 1-36), providing the potential for αS monomers to interact with either the N- or C-termini of the fibrils (Figure 7). We therefore propose that the initial monomer–aggregate interactions occur between the intrinsically disordered monomer N-terminus and intrinsically disordered regions of the aggregates.

The specificity of monomer–aggregate interactions at the termini is consistent with previous work by our laboratory (50, 51) and others (52, 53) on αS monomer–monomer interactions, which showed that transient IDP–IDP dimers are mediated by N–N or N–C terminal interactions. Recent in vitro and in cell studies have shown that both the N- and C-termini of αS influence the amyloid growth kinetics, morphologies of resultant fibrils, and capacity for seeding full-length

αS (25-27). Consistent with our observations, previous work has shown that fibril seeds with an N-terminal truncation are less efficient seeding templates (25), which may be due to reduced monomer recruitment by truncated N-terminal IDRs based on the present hypothesis. C-terminally truncated αS has variable seeding effects on full-length αS in both aggregation kinetics and morphologies, depending upon the truncation length (25-27). This highlights the complex roles the disordered termini play in the aggregation of αS, both in the initiation of amyloid formation and regulation of amyloid structures and morphologies.

The results presented in this work shed new light on the role of the IDRs in the amyloid seeding mechanism. In the case of Ac-αS, we propose that the first step in the seeding mechanism is monomer recruitment by the fibril IDRs (Figure 7). Once at the surface, monomers can template onto the fibril through elongation, or nucleate on the fibril surface through secondary nucleation (10, 31). Under the conditions used here, near neutral pH and higher ionic strength, elongation is the predominant mechanism over surface-mediated secondary nucleation (54). The ability to template on the fibril is dependent on an accessible structured core (55), the core dynamics (21, 56), and the orientation of the monomer–fibril interaction. Previous work from our group has shown that increased dynamics in the core reduces the seeding capacity of αS fibrils (56), and that N–N, rather than N–C, monomer interactions promote fibril formation (50). Thus, while both fibrils and off-pathway oligomers are able to recruit monomers with their IDRs, only fibrils are able to seed amyloid formation under these conditions (Figure 7) because the oligomers lack a core amenable to templating and cannot interact with monomers in an N–N orientation. Taking in to consideration the results of past and present work, we propose a multi-step Ac-αS seeding mechanism that highlights the complex role of dynamics and disorder: 1) monomers are recruited by fibril IDRs through N–N monomer–fibril interactions and 2) a rigid and accessible fibril core provides efficient templating for fibril elongation. This proposed mechanism suggests a critical role for the fibril IDR in monomer recruitment to the fibril surface and establishes the intrinsically disordered termini, especially the N-terminus, as potential targets for interrupting pathological αS amyloidogenesis. Thus, future therapeutic approaches to fibril inhibition should not ignore targeting of the IDRs that coat the surface in order to block monomer recruitment and re-association with the fibril.

4. Materials and Methods

Protein expression and purification

N-terminally acetylated human αS was obtained through co-expression with the pNatB plasmid (Addgene #53613) in *E. coli* BL21(DE3) cells. Uniformly ^{15}N-labeled Ac-αS for NMR was expressed in M9 minimal media with ^{15}N-ammonium chloride as the only nitrogen source. [U-^{15}N]-Ac-αS was purified as previously described (57). Protein purity and molecular weight were confirmed by ESI-MS. Protein was stored as lyophilized powder at -20°C until usage.

Preparation of stable off-pathway oligomers and fibrils

Off-pathway oligomers were prepared by dissolving 10 mg Ac-αS lyophilized powder in 1 mL 10 mM PBS buffer (pH 7.4) and incubating the protein solution at 37°C for 5 hours with shaking at 300 rpm. The sample was then loaded on a Superose 6 size exclusion column (GE Healthcare) and eluted with PBS buffer at a flow rate of 0.3 ml/min at 4°C. Oligomer samples were concentrated with 3 kDa centrifugal filter units (Millipore Sigma) and were kept in 4°C until use.

All oligomer samples were used within 24 hours. Fibrils were prepared as previous described (56). In short, protein powder was dissolved in 10 mM PBS (pH 7.4), and large aggregates were removed through centrifugal filtration using a 50 kDa molecular weight cutoff (Millipore Sigma). Fibrils were prepared by incubating 100 μL of 70 μM Ac-αS with a single Teflon bead (3 mm, Saint-Gobain N.A.) at 37°C, shaking at 600 rpm in 96-well clear bottom plates (Corning) in a POLARstar Omega fluorimeter (BMG Labtech) for at least 72 hours. Fibrils were washed multiple times with 10 mM PBS (pH 7.4) by re-suspension and centrifugation at 20k rpm for 30 mins in order to remove residual soluble and non-fibrillar components. Oligomer and fibril concentrations were measured by UV 280 nm after denaturation with 4 M guanidine hydrochloride.

Thioflavin T seeding experiments

Ac-αS protein powder was dissolved in 10 mM PBS (pH 7.4) and filtered through 50 kDa centrifugal units to remove large aggregates formed during lyophilization. Different concentrations of fibril seeds or off-pathway oligomers were added to 70 μM monomer solutions with 20 μM ThT. To obtain varying lengths of fibril seeds, probe sonication was applied to the fibril seeds with 30% power. Morphologies and length distributions of sonicated fibrils were assessed by TEM. For each condition, 100 μL solution was dispensed into clear bottom 96-well plates and sealed with Axygen sealing tape (Corning). The plates were incubated at 37°C in a POLARstar Omega fluorimeter (BMG Labtech) under quiescent conditions. Fluorescence was monitored every 33 mins for at least 5 days.

Transmission Electron Microscope (TEM)

3.5 μL samples were applied to carbon coated cooper grids (Electron Microscopy Sciences) and incubated at room temperature for 90 s. Excessive solution on the grid was removed by gently tapping with filter paper. 3.5 μL 3% uranyl acetate solution (Fisher Scientific) was then added to the grid and incubated at room temperature for 60 s. The grid was then washed twice with 3.5 μL ultrapurified water. Images were recorded with a JEOL 1200EX electron microscope with 80k voltage.

Circular Dichroism (CD)

Far-UV wavelength spectra of off-pathway oligomers and fibrils were measured on an AVIV 420SF CD spectrophotometer (AVIV Biomedical Inc.) in a 1 mm pathlength quartz cuvette at 25°C. Samples were diluted in 10 mM PBS (pH 7.4).Wavelength scans were obtained from 200–260 nm with a step size of 1 nm and 10 s averaging time.

NMR experiments

All NMR experiments were performed in 10 mM PBS (pH 7.4) with 10% D_2O at 4°C. To prepare [U-^{15}N]-Ac-αS monomer samples, lyophilized protein powder was dissolved in PBS buffer (pH 7.4), and large aggregates were removed using a 50 kDa centrifugal filter. In order to detect [U-^{15}N]-Ac-αS fibrils by NMR, the fibrils were sonicated on ice by probe sonicator at 30% power level with four cycles of 30 s power on and 30 s power off. Fibril morphologies were checked by TEM before and after NMR experiments. All [U-^{15}N]-Ac-αS samples were concentrated to working concentrations in 3 kDa centrifugal filters. All concentrations reported are in monomer equivalents as determined by a BCA assay.

Relaxation experiments. For all samples, ^{15}N transverse relaxation (R_2) experiments were measured from a series of HSQC-based 2D ^{1}H–^{15}N spectra using the Carr-Purcell-Meiboom-Gill pulse sequence with varying relaxation delays: ^{15}N-Ac-αS sonicated fibrils and ^{15}N-Ac-αS monomers at 800 MHz- 0, 8, 16, 16, 32, 64, 128, 192, 256, and 320 ms; ^{15}N-Ac-αS off-pathway oligomers and ^{15}N-Ac-αS monomers at 800 MHz- 8, 16, 32, 48, 64, 96, 128, 160, 192, 224, and 256 ms; ^{15}N-Ac-αS monomers alone or in the presence of sonicated fibrils at 700 MHz- 0, 8, 16, 32, 32, 64, 128, 192, 256, 320 ms; and ^{15}N-Ac-αS monomers alone or in the presence of off-pathway oligomers at 700 MHz- 8, 16, 32, 48, 64, 96, 128, 160, 192, 224, and 256 ms. ^{15}N-R_2 rates were measured by fitting a single exponential decay function to peak intensities of the decay curves for each residue. Where reported, ΔR_2 is the difference between the measured ^{15}N-R_2 of the indicated sample and the ^{15}N-R_2 of pure [U-^{15}N]-Ac-αS monomer at the same concentration. In the ^{15}N-R_2 Hahn echo experiments(58) on ^{15}N-Ac-αS sonicated fibrils and ^{15}N-Ac-αS monomers at 800 MHz, the following relaxation delays were used: 0.768, 3.84, 7.68, 7.68, 19.2, 38.4, 76.8, 115, 154, and 230 ms. The conformational exchange contribution to R_2 (R_{ex}) was determined for each residue as: $R_{ex} = R_2^{HE} - R_2$, where R_2^{HE} is the apparent relaxation rate derived from the ^{15}N-R_2 Hahn echo experiment.

^{15}N-DEST experiments. ^{15}N-DEST experiments were conducted by applying an ^{15}N RF saturation pulse of 350 Hz or 150 Hz for 900 ms at variable ^{15}N-frequency offsets: 350 μM ^{15}N-Ac-αS monomer at 800 MHz- 0, ±0.5, ±1, ±2, ±4, ±8, ±18, and ±30 kHz; 350 μM ^{15}N-Ac-αS sonicated fibril at 800 MHz- 0, ±0.5, ±1, ±2, ±4, -8, +18, and ±30 kHz; and 90 μM ^{15}N-Ac-αS monomer in the absence or presence of 90 μM Ac-αS fibril seed at 700 MHz: 0, ±0.5, ±1, ±4, and ±30 kHz. For each sample, a reference experiment in which 0 Hz RF saturation was applied at an ^{15}N-offset of +30 kHz was also conducted. ^{15}N-DEST profiles were obtained for each residue as peak intensity vs. ^{15}N-offset. The ΔΘ profile was derived by calculating a Θ value for each residue, where $\Theta = \frac{(I_{30kHz}+I_{-30kHz})-(I_{1kHz}+I_{-1kHz})}{(I_{30kHz}+I_{-30kHz})}$, and calculating ΔΘ as $\Delta\Theta = \Theta_{+fibrils} - \Theta_{-fibrils}$. The residue-specific ΔR_2 and DEST profiles of the ^{15}N-Ac-αS sonicated fibril sample and ^{15}N-Ac-αS monomer in the presence of sonicated fibril seeds were fit simultaneously to the McConnell equations using a simple two-state model in the DESTfit program (33, 34) to extract $p_{visible}$, k_{on}^{app}, and R_2^{bound}. The DEST profiles of 350 μM ^{15}N-Ac-αS monomer were fit to a model in which the NMR-detectable state was not in exchange with the invisible state ($k_{on}^{app} = 0\ s^{-1}$) as a control.

Cell culture

Human SH-SY5Y neuroblastoma cells (ATCC) were cultured in DMEM/F12 (GE Healthcare) with 10% fetal bovine serum (FBS, Gibco Co.) and kept in a 5% CO_2 humidified atmosphere at 37°C. Cells were seeded onto 96-well (Corning) or 12-well glass bottom plates (Cellvis) for cell viability or immunocytochemistry experiments, respectively. Cells were allowed to recover for at least 24 hours, at which point they reached 75% confluency, before conducting experiments.

Cell viability MTS reduction assay

Cells were treated with different concentrations of fibrils or oligomers for 24 hours. Following the manufacturer's instructions, 20 μL 3-(4, 5-dimethylthiazol-2-yl)-5-(3-carboxymethoxyphenol)-2-(4-sulfophenyl)-2H-tetrazolium reaction solution (MTS, Promega) was added to 100 μL cell culture and incubated for 2 hours at 37°C. Cell viability was measured

as absorbance at 490 nm, which is directly proportional to the number of living cells in the culture.

Immunocytochemistry

Ac-αS samples (monomer, oligomers, and fibrils) were labeled with fluorescent ATTO488-NHS-ester (ATTO-TEC GmbH) per the manufacturer's procedure. In brief, samples were incubated with a 2 M excess of ATTO488-NHS-ester in labeling buffer (PBS/sodium bicarbonate solution, pH 8.3) for 1 h at room temperature. Unreacted fluorophore was washed from the conjugated ATTO488-fibrils by centrifugation at 20k rpm for 30 min and resuspension of the ATTO488-fibril pellet in fresh 10 mM PBS (pH 7.4); this washing procedure was repeated twice. Unbound fluorophore was washed from monomers and oligomers three times with 10 mM PBS (pH 7.4) by filtration with 3 kDa centrifugal units. Cells were treated with 3 μM ATTO488-Ac-αS monomers, oligomers, or fibrils and incubated for 24 hours.

Cells were fixed with 10% formalin (Sigma Aldrich) and permeabilized in PBS buffer with 0.5% Triton. Before being incubated with antibodies, cells were blocked with 5% Donkey Serum solution (Sigma Aldrich) for 30 min at 37°C. Cells were incubated with primary antibody (SYN-1, BD Biosciences) at 4°C overnight and protected from light. Afterwards, cells were washed with 10 mM PBS (pH 7.4) three times and incubated with fluorophore-conjugated secondary antibody (TRITC antibody, Sigma Aldrich) at room temperature for 1 h. Cell nuclei were stained with 4', 6-diamidino-2-phenylindole (DAPI, Millipore Sigma) for 90s and washed with PBS. All samples were imaged by a Zeiss LSM 780 confocal laser scanning microscope. Image analysis was done by Fiji (ImageJ) (59).

Data Availability

All data and protocols are available in the main text or the SI Appendix. Further inquiries can be addressed to the corresponding author.

Acknowledgements

We thank Dr. M. Maral Mouradian (Rutgers Robert Wood Johnson Medical School) for access to cell culture equipment and materials and lab members for experimental assistance. This work was funded by NIH grant GM110577 to J.B.

Competing Interests

The authors declare no competing interests.

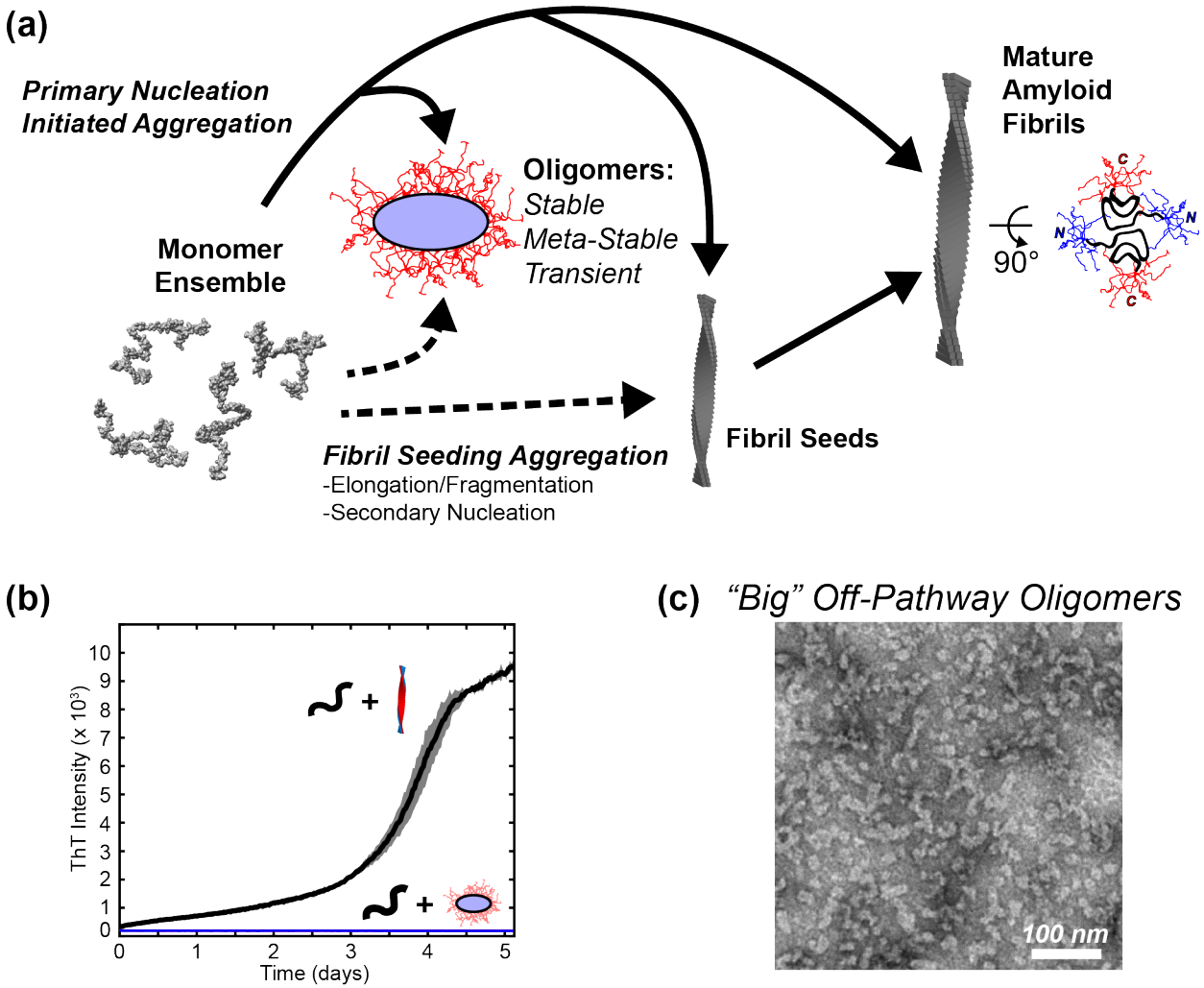

Figure 1. (a) In vitro aggregation of αS can be broken into two categories of amyloid fibril formation. The first, primary nucleation (solid arrows), is a stochastic process whereby an initial nucleus of amyloid competent αS monomers is formed and is most likely a heterogenous nucleation process (i.e. nucleation at a surface), both in vitro and in vivo, rather than a homogenous process occurring in bulk solution. The second category is comprised of two "secondary" processes (dashed arrows): fibril fragmentation/elongation and secondary nucleation. Elongation involves the templated addition of monomers to the ends of existing fibrils; fragmentation contributes to this process by increasing available ends through breaking of existing fibrils. Secondary nucleation is a type of heterogenous nucleation that specifically involves the nucleation of monomers at the surface of existing fibrils. The solution conditions have been shown to heavily influence which of these categories is favored during amyloid fibril formation. (b) In an in vitro ThT fibril seeding assay at 37°C, pre-formed Ac-αS fibrils induce the formation of new amyloid fibrils (black- 1 μM seeds, 40 μM monomer). However, stable big off-pathway oligomers do not have the ability to induce formation of new amyloid fibrils (blue- 1 μM seeds, 40 μM monomer). (c) A TEM image of isolated big off-pathway oligomers displays their worm-like morphology.

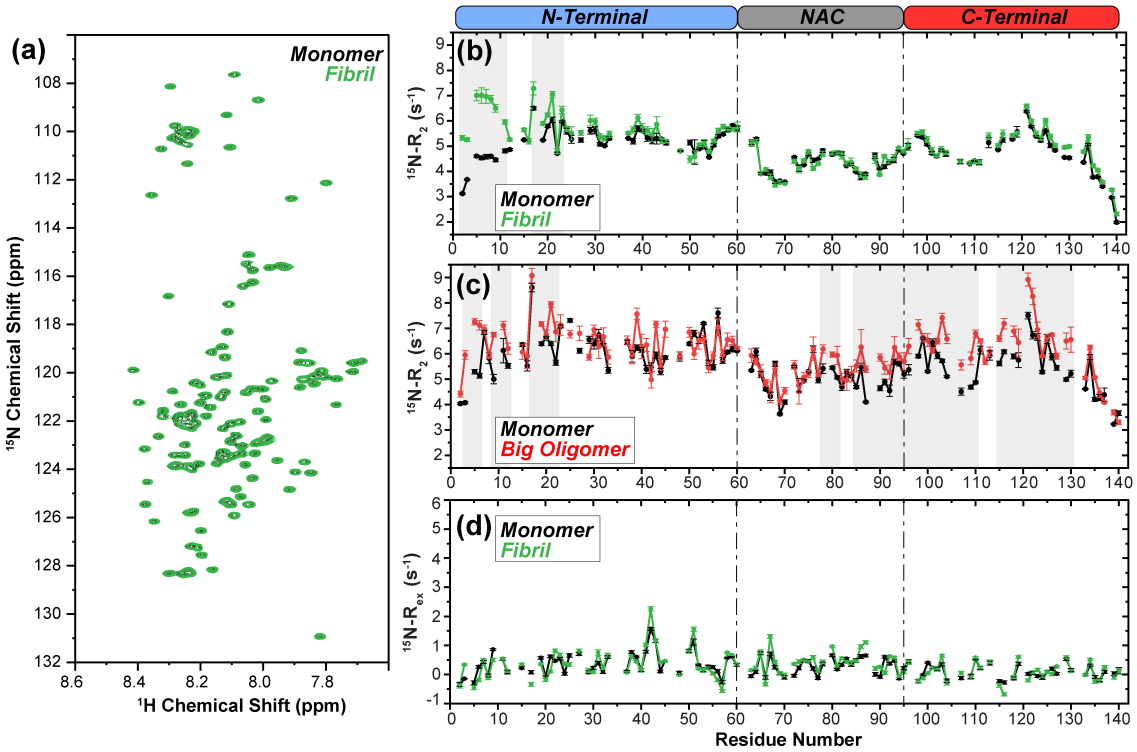

Figure 2. (a) ^{1}H–^{15}N HSQC spectra of 350 μM [U-^{15}N]-Ac-αS monomer (black) and 350 μM [U-^{15}N]-Ac-αS sonicated fibrils (green). An overlay of these spectra shows that there is no difference in chemical shifts or linewidths, indicating that the detected species in the [U-^{15}N]-fibrils sample is actually monomer dissociated from fibrils. (b,c) Residue-level ^{15}N-transverse relaxation rates (^{15}N-R_2) of (b) 350 μM [U-^{15}N]-Ac-αS monomers (black) and 350 μM [U-^{15}N]-Ac-αS sonicated fibrils (green) and (c) 350 μM [U-^{15}N]-Ac-αS monomers (black) and 350 μM [U-^{15}N]-Ac-αS big oligomers (red). The three sequential domains of αS are indicated on top (N-terminal, blue; NAC, gray; and C-terminal, red). Dashed lines separate the domains within the plot. Regions of three or more consecutive residues that have a ΔR_2 between the monomer and aggregate samples ≥ 0.5 s^{-1} are highlighted in gray. (d) Relaxation exchange rates (^{15}N-R_{ex}) as measured by ^{15}N-R_2 Hahn echo experiments of 350 μM [U-^{15}N]-Ac-αS monomers (black) and 350 μM [U-^{15}N]-Ac-αS sonicated fibrils (green). No substantial contribution of R_{ex} is observed in either sample. The error bars in the relaxation data are propagated from the single exponential decay fitting errors of the underlying ^{15}N-R_2 data. All NMR data were acquired in PBS, pH 7.4 and 4°C at 800 MHz ^{1}H Larmor frequency.

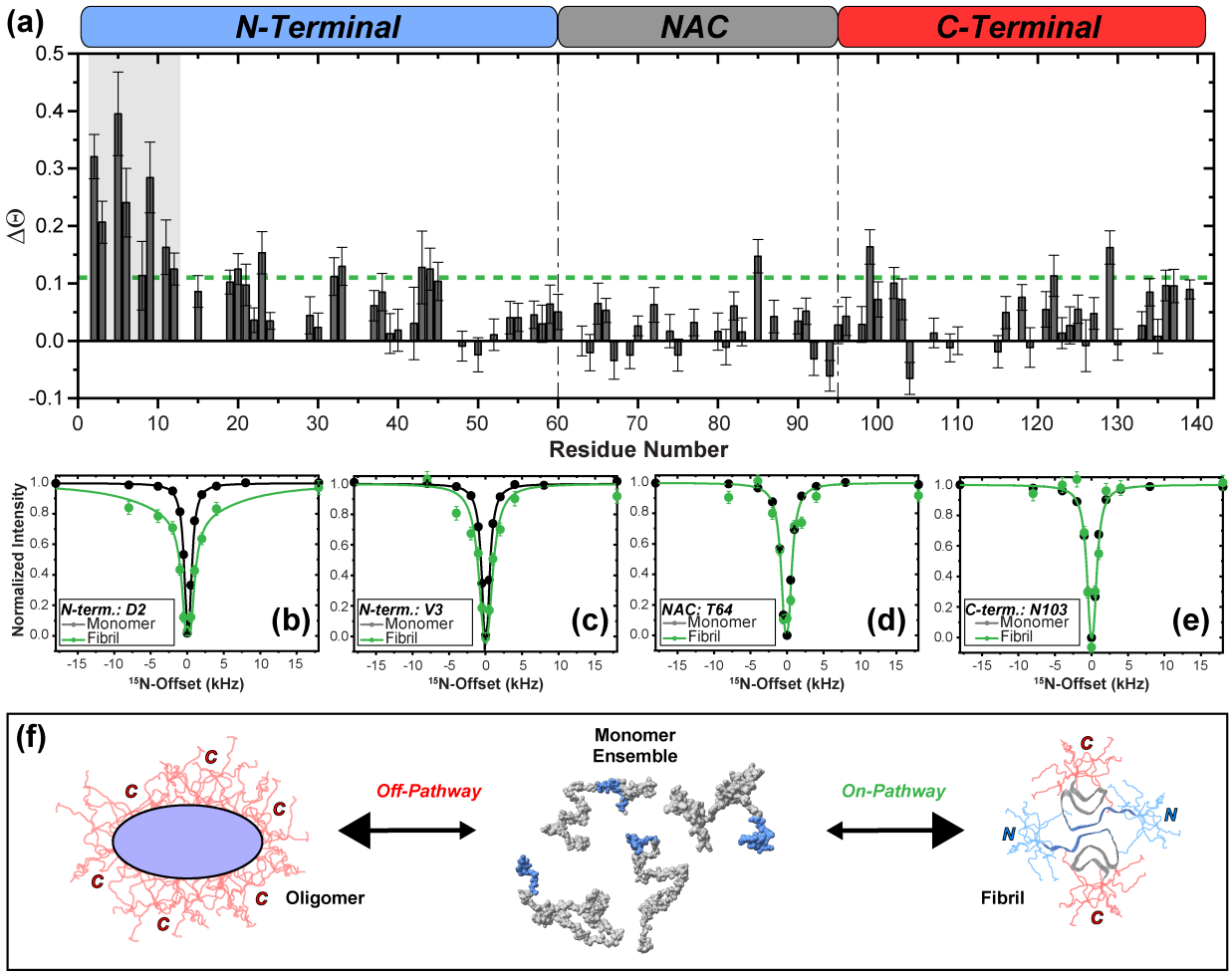

Figure 3. Identifying direct contacts of Ac-αS monomers with fibrils. (a) ΔΘ calculated as the difference in Θ between ^{15}N-Ac-αS sonicated fibrils and ^{15}N-Ac-αS monomers derived from ^{15}N-DEST intensities at ±30 kHz and ±1 kHz ^{15}N-offsets with a 350 Hz saturation frequency. Regions of consecutive residues with ΔΘ higher than 0.11 (green dashed line), where broadening of the residue-specific DEST profiles is observed, are highlighted in gray. The three linear αS domains are indicated on the top. (b–e) Examples of ^{15}N-DEST profiles with 350 Hz saturation frequency of 350 μM ^{15}N-Ac-αS monomer (black) or 350 μM ^{15}N-sonicated Ac-αS fibrils (green). Experimental data points are shown as symbols. Fit curves using a two-state exchange model are shown as solid lines. N-terminal residues D2 and V3 show broadening of the DEST profiles in the sonicated fibrils sample (b–c), whereas residues in the NAC (T64) and C-terminal (N103) do not show this effect (d–e). Error bars are derived from the noise of the underlying 2D spectra. All experiments were conducted in PBS, pH 7.4, 4°C at 800 MHz ^{1}H Larmor frequency. (f) Depiction of the equilibrium between monomers and the ^{15}N-labeled higher order aggregates, which results in populations of ^{15}N-labeled monomers being the dominant species detected in HSQC spectra. N- (blue) and C-terminal (red) domains are indicated in the fibril and oligomer schematics. The N-terminal region that shows the greatest ^{15}N-R_2 perturbation in both aggregates and DEST enhancement in the fibrils is indicated in blue in the monomer.

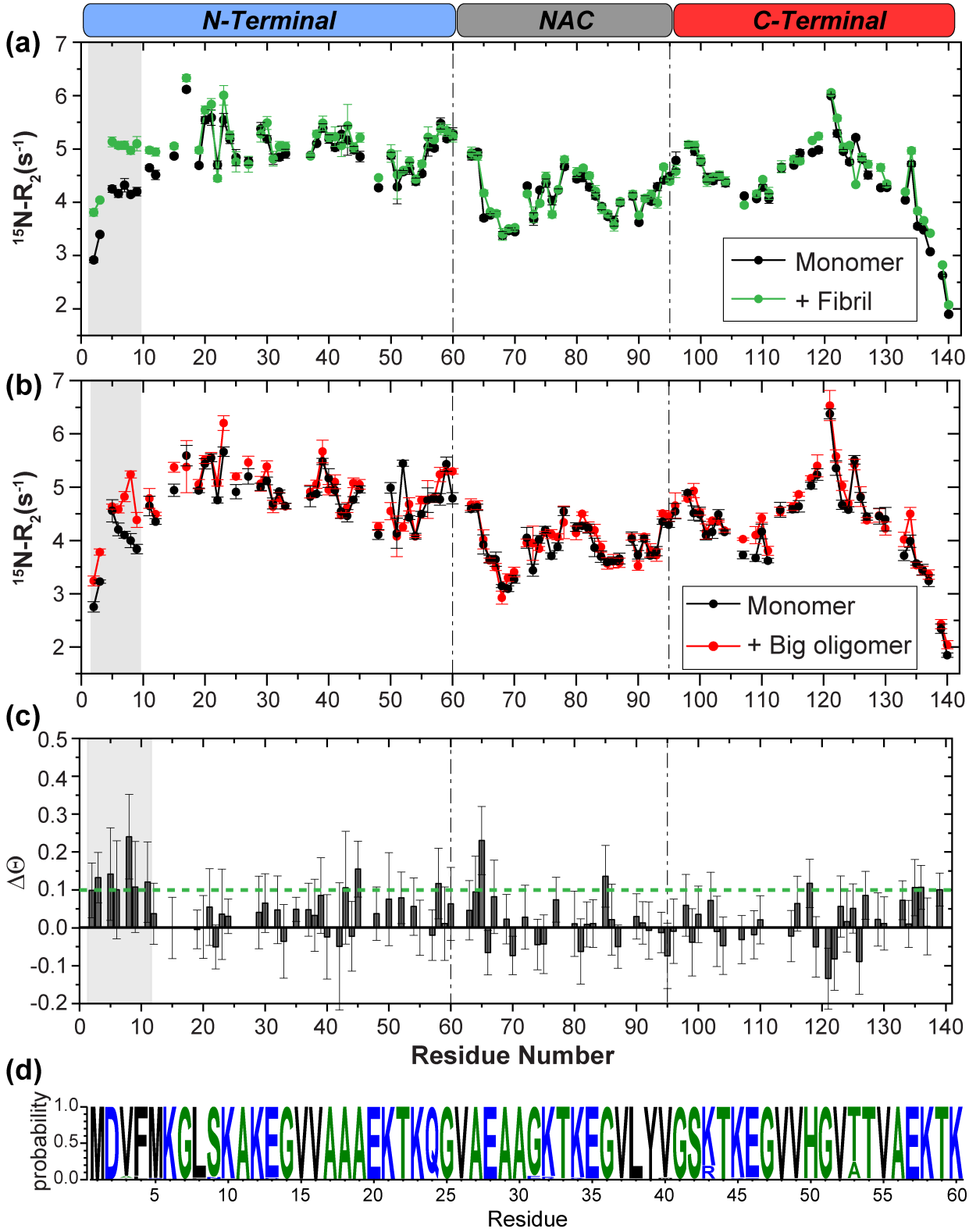

Figure 4. Perturbation to [U-^{15}N]-Ac-αS monomers in the presence of fibril or oligomer aggregates. Residue-level ^{15}N-R$_2$ of (a) green: 90 μM [U-^{15}N]-Ac-αS monomer + unlabeled fibril

(1:1 molar ratio) and black: 90 μM [U-^{15}N]-Ac-αS monomer alone, and (b) red: 90 μM [U-^{15}N]-Ac-αS monomer + unlabeled big oligomers (1:1 molar ratio) and black: 90 μM [U-^{15}N]-Ac-αS monomer alone. The error bars are propagated from the single exponential decay fitting errors. Regions of three or more consecutive residues that have a ΔR_2 between monomers in the presence and absence of aggregates $\geq 0.5\ s^{-1}$ are highlighted in gray. (c) ΔΘ calculated as the difference in Θ between ^{15}N-Ac-αS monomers in the presence or absence of Ac-αS sonicated fibril seeds derived from ^{15}N-DEST intensities at ±30 kHz and ±1 kHz ^{15}N-offsets with a 350 Hz saturation frequency. Regions of consecutive residues with ΔΘ higher than 0.10 (green dashed line), mean +1 standard deviation, are highlighted in gray. Error bars are propagated from the noise levels of each 2D spectrum. All NMR data were acquired at 700 MHz ^{1}H Larmor frequency. (d) Sequence logo alignment (60) of the first 60 residues of αS sequences, constructed using ~230 unique αS sequences found in the NCBI Protein database and created using WebLogo (61), showing the high conservation of the N-terminal domain. Colors designate hydrophobicity, where black= hydrophobic, blue= charged, and green= neutral.

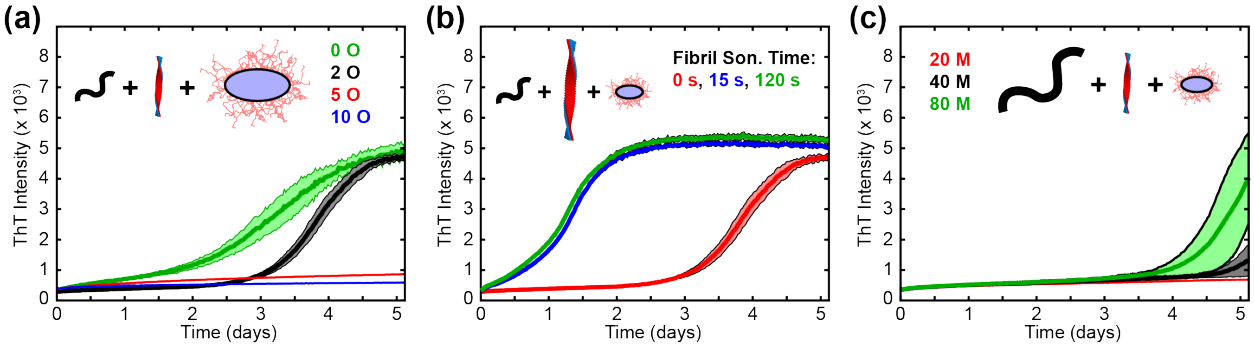

Figure 5. Thioflavin T fluorescence assays of Ac-αS seeded aggregation under various conditions of the reaction components. (a) Seeded aggregation of 40 μM monomer, 1 μM (monomer equivalent) fibril, and either 0 μM (green), 2 μM (black), 5 μM (red), or 10 μM (blue) big oligomers. (b) Seeded aggregation of 40 μM monomer, 1 μM fibril, and 2 μM big oligomer, where the fibril seeds are sonicated for either 0 s (red), 15 s (blue), or 120 s (green) before addition to the reaction. (c) Seeded aggregation of either 20 μM (red), 40 μM (black), or 80 μM (green) monomer, with 1 μM fibril and 2 μM big oligomer.

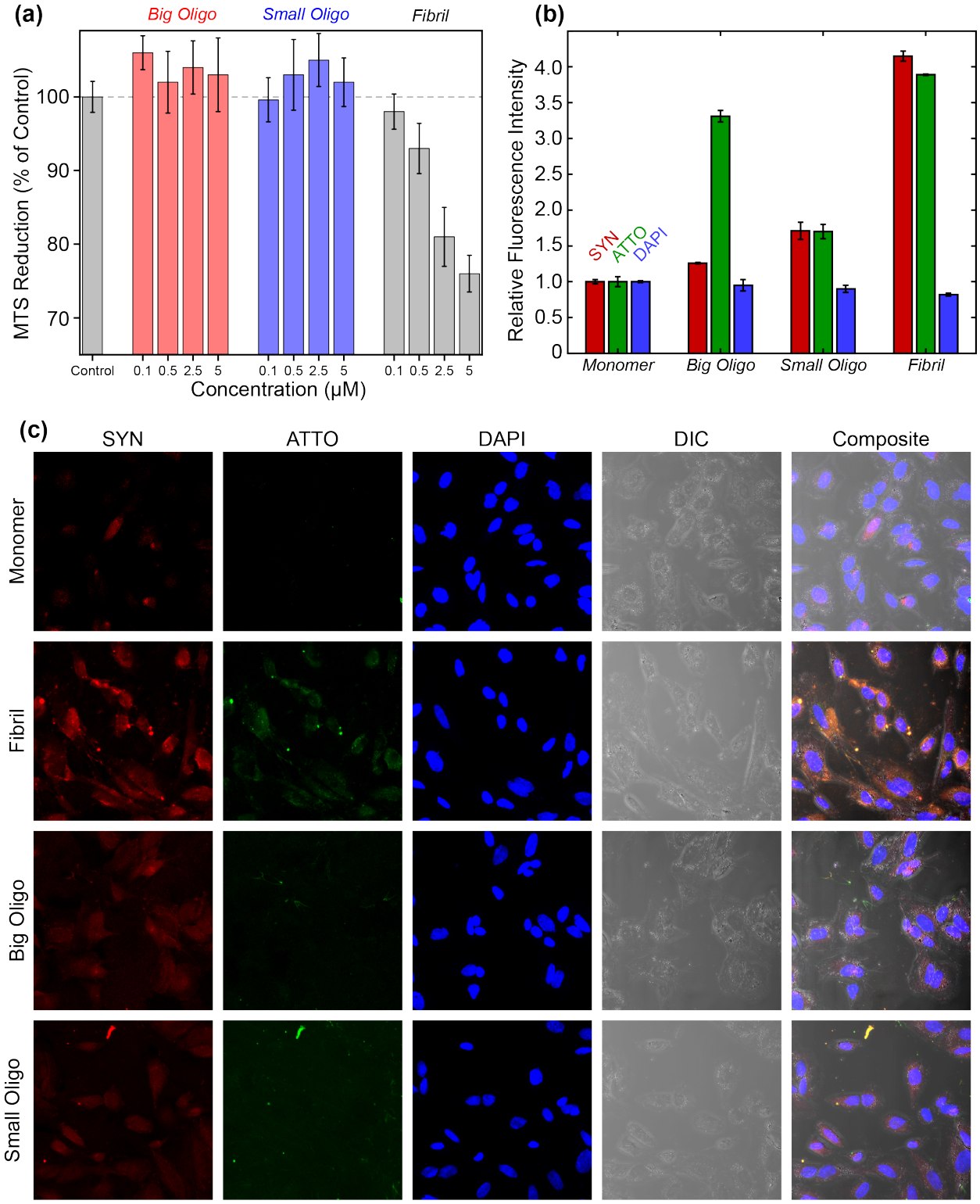

Figure 6. (a) Cell viability assessed using an MTS reduction assay. Both big and small oligomers show no reductions in cell viability with increasing concentrations, while increasing concentrations of Ac-αS fibrils show a dose-dependent reduction in cell viability. (b) Quantitation of the relative fluorescence intensities observed from the (c) confocal fluorescence

images, with SH-SY5Y cells treated with either monomer, fibril, big oligomer, or small oligomer, and then stained with anti-αS -antibody, ATTO dye, or DAPI.

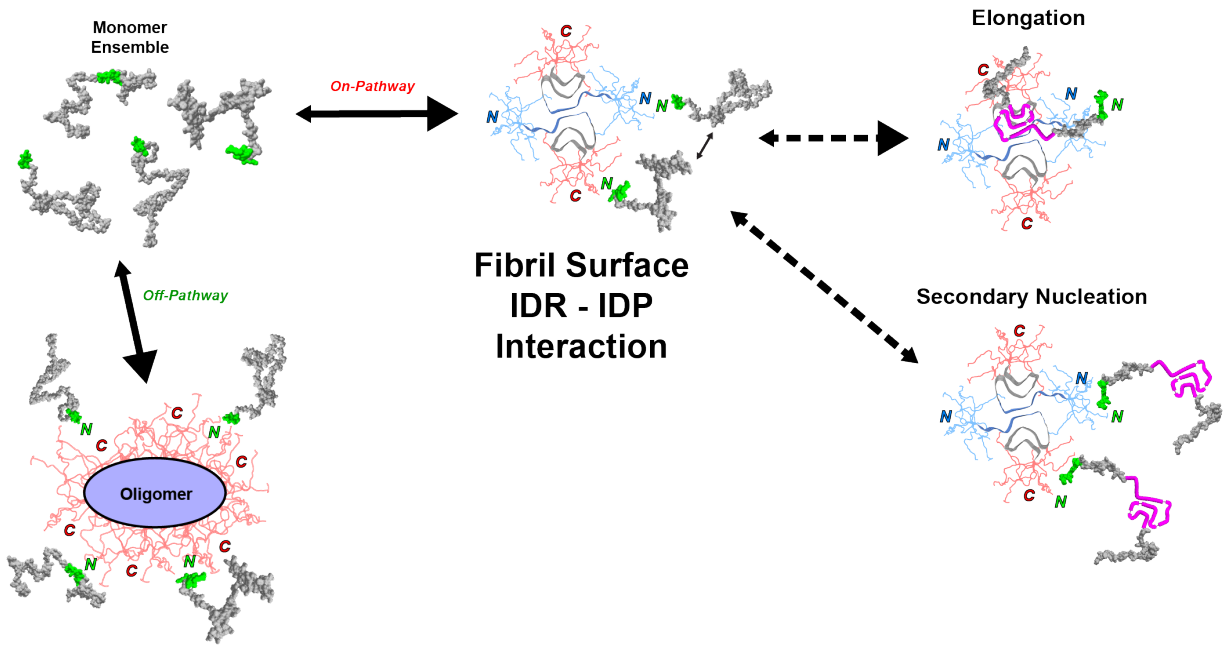

Figure 7. In solution, αS exists as an ensemble of inter-converting monomers with different conformations. αS can sample aggregation-competent conformations that lead to the aggregation of multiple monomers into oligomers and amyloid fibrils. These aggregates can adopt structures that will not form amyloid fibrils ("off-pathway") or adopt structures that will eventually form amyloid fibrils ("on-pathway"). In either case, these aggregate species are in equilibrium with monomeric species in solution. The intrinsically disordered monomers can interact via the N-terminal hotspot (green) with the intrinsically disordered regions (N-terminus, blue and/or C-terminus, red) of the amyloid fibril species to elongate the fibrils (elongation) or nucleate with other surface-associated monomer species to form new fibrils (secondary nucleation). The association of the N-terminal hotspot of αS monomers with the intrinsically disordered C-terminus of off-pathway oligomers does not induce fibril or further oligomer formation.

References

1. F. Chiti, C. M. Dobson, Protein Misfolding, Amyloid Formation, and Human Disease: A Summary of Progress Over the Last Decade. *Annu Rev Biochem* **86**, 27-68 (2017).

2. H. A. Lashuel, C. R. Overk, A. Oueslati, E. Masliah, The many faces of alpha-synuclein: from structure and toxicity to therapeutic target. *Nat Rev Neurosci* **14**, 38-48 (2013).

3. A. L. Mahul-Mellier *et al*., Fibril growth and seeding capacity play key roles in alpha-synuclein-mediated apoptotic cell death. *Cell Death Differ* **22**, 2107-2122 (2015).

4. F. van Diggelen *et al*., Two conformationally distinct alpha-synuclein oligomers share common epitopes and the ability to impair long-term potentiation. *PLoS One* **14**, e0213663 (2019).

5. G. Fusco *et al*., Structural basis of membrane disruption and cellular toxicity by alpha-synuclein oligomers. *Science* **358**, 1440-1443 (2017).

6. S. W. Chen *et al*., Structural characterization of toxic oligomers that are kinetically trapped during alpha-synuclein fibril formation. *Proc Natl Acad Sci U S A* **112**, E1994-2003 (2015).

7. N. Cremades *et al*., Direct observation of the interconversion of normal and toxic forms of alpha-synuclein. *Cell* **149**, 1048-1059 (2012).

8. B. K. Choi *et al*., Large alpha-synuclein oligomers inhibit neuronal SNARE-mediated vesicle docking. *Proc Natl Acad Sci U S A* **110**, 4087-4092 (2013).

9. T. Scheidt *et al*., Secondary nucleation and elongation occur at different sites on Alzheimer's amyloid-beta aggregates. *Sci Adv* **5**, eaau3112 (2019).

10. R. Gaspar *et al*., Secondary nucleation of monomers on fibril surface dominates alpha-synuclein aggregation and provides autocatalytic amyloid amplification. *Q Rev Biophys* **50**, e6 (2017).

11. D. Pinotsi *et al*., Nanoscopic insights into seeding mechanisms and toxicity of alpha-synuclein species in neurons. *Proc Natl Acad Sci U S A* **113**, 3815-3819 (2016).

12. N. Bengoa-Vergniory, R. F. Roberts, R. Wade-Martins, J. Alegre-Abarrategui, Alpha-synuclein oligomers: a new hope. *Acta Neuropathol* **134**, 819-838 (2017).

13. G. Mercado, N. Lopez, A. Martinez, S. P. Sardi, C. Hetz, A new model to study cell-to-cell transfer of alphaSynuclein in vivo. *Biochem Biophys Res Commun* **503**, 1385-1393 (2018).

14. H. T. Lam, M. C. Graber, K. A. Gentry, J. Bieschke, Stabilization of alpha-Synuclein Fibril Clusters Prevents Fragmentation and Reduces Seeding Activity and Toxicity. *Biochemistry* **55**, 675-685 (2016).

15. C. M. Cremers *et al*., Polyphosphate: A Conserved Modifier of Amyloidogenic Processes. *Mol Cell* **63**, 768-780 (2016).

16. E. D. Agerschou *et al*., An engineered monomer binding-protein for alpha-synuclein efficiently inhibits the proliferation of amyloid fibrils. *Elife* **8**, e46112 (2019).

17. N. Lorenzen *et al*., The role of stable alpha-synuclein oligomers in the molecular events underlying amyloid formation. *J Am Chem Soc* **136**, 3859-3868 (2014).

18. M. D. Tuttle *et al*., Solid-state NMR structure of a pathogenic fibril of full-length human alpha-synuclein. *Nat Struct Mol Biol* **23**, 409-415 (2016).

19. R. Guerrero-Ferreira *et al*., Cryo-EM structure of alpha-synuclein fibrils. *Elife* **7**, e36402 (2018).

20. B. Li *et al*., Cryo-EM of full-length alpha-synuclein reveals fibril polymorphs with a common structural kernel. *Nat Commun* **9**, 3609 (2018).

21. K. Zhao *et al*., Parkinson's disease associated mutation E46K of α-synuclein triggers the formation of a distinct fibril structure. *Nat Commun* **11**, 2643 (2020).

22. M. Schweighauser *et al*., Structures of α-synuclein filaments from multiple system atrophy. *Nature* 10.1038/s41586-020-2317-6 (2020).

23. S. Sangwan *et al*., Inhibition of synucleinopathic seeding by rationally designed inhibitors. *Elife* **9**, e46775 (2020).

24. V. V. Shvadchak, K. Afitska, D. A. Yushchenko, Inhibition of alpha-Synuclein Amyloid Fibril Elongation by Blocking Fibril Ends. *Angew Chem Int Ed Engl* **57**, 5690-5694 (2018).

25. M. Terada *et al*., The effect of truncation on prion-like properties of alpha-synuclein. *J Biol Chem* **293**, 13910-13920 (2018).

26. Z. A. Sorrentino *et al*., Physiological C-terminal truncation of alpha-synuclein potentiates the prion-like formation of pathological inclusions. *J Biol Chem* **293**, 18914-18932 (2018).

27. Z. A. Sorrentino *et al*., Carboxy-terminal truncation and phosphorylation of alpha-synuclein elongates survival in a prion-like seeding mouse model of synucleinopathy. *Neurosci Lett* 10.1016/j.neulet.2020.135017, 135017 (2020).

28. K. Vamvaca, M. J. Volles, P. T. Lansbury, Jr., The first N-terminal amino acids of alpha-synuclein are essential for alpha-helical structure formation in vitro and membrane binding in yeast. *J Mol Biol* **389**, 413-424 (2009).

29. M. Runfola, A. De Simone, M. Vendruscolo, C. M. Dobson, G. Fusco, The N-terminal Acetylation of alpha-Synuclein Changes the Affinity for Lipid Membranes but not the Structural Properties of the Bound State. *Sci Rep* **10**, 204 (2020).

30. M. D. Watson, J. C. Lee, N-Terminal Acetylation Affects alpha-Synuclein Fibril Polymorphism. *Biochemistry* **58**, 3630-3633 (2019).

31. A. K. Buell *et al*., Solution conditions determine the relative importance of nucleation and growth processes in alpha-synuclein aggregation. *Proc Natl Acad Sci U S A* **111**, 7671-7676 (2014).

32. N. Lorenzen *et al*., How epigallocatechin gallate can inhibit alpha-synuclein oligomer toxicity in vitro. *J Biol Chem* **289**, 21299-21310 (2014).

33. N. L. Fawzi, J. Ying, R. Ghirlando, D. A. Torchia, G. M. Clore, Atomic-resolution dynamics on the surface of amyloid-beta protofibrils probed by solution NMR. *Nature* **480**, 268-272 (2011).

34. N. L. Fawzi, J. Ying, D. A. Torchia, G. M. Clore, Probing exchange kinetics and atomic resolution dynamics in high-molecular-weight complexes using dark-state exchange saturation transfer NMR spectroscopy. *Nat Protoc* **7**, 1523-1533 (2012).

35. J. W. Brown *et al*., beta-Synuclein suppresses both the initiation and amplification steps of alpha-synuclein aggregation via competitive binding to surfaces. *Sci Rep* **6**, 36010 (2016).

36. P. Alam, L. Bousset, R. Melki, D. E. Otzen, alpha-synuclein oligomers and fibrils: a spectrum of species, a spectrum of toxicities. *J Neurochem* **150**, 522-534 (2019).

37. L. Pieri, K. Madiona, L. Bousset, R. Melki, Fibrillar alpha-synuclein and huntingtin exon 1 assemblies are toxic to the cells. *Biophys J* **102**, 2894-2905 (2012).

38. E. Luna *et al*., Differential alpha-synuclein expression contributes to selective vulnerability of hippocampal neuron subpopulations to fibril-induced toxicity. *Acta Neuropathol* **135**, 855-875 (2018).

39. E. Colla *et al*., Accumulation of toxic alpha-synuclein oligomer within endoplasmic reticulum occurs in alpha-synucleinopathy in vivo. *J Neurosci* **32**, 3301-3305 (2012).

40. B. Winner *et al*., In vivo demonstration that alpha-synuclein oligomers are toxic. *Proc Natl Acad Sci U S A* **108**, 4194-4199 (2011).

41. C. A. Waudby *et al*., The interaction of alphaB-crystallin with mature alpha-synuclein amyloid fibrils inhibits their elongation. *Biophys J* **98**, 843-851 (2010).

42. N. Carulla *et al*., Molecular recycling within amyloid fibrils. *Nature* **436**, 554-558 (2005).

43. K. Afitska, A. Fucikova, V. V. Shvadchak, D. A. Yushchenko, alpha-Synuclein aggregation at low concentrations. *Biochim Biophys Acta Proteins Proteom* **1867**, 701-709 (2019).

44. D. Hall, J. Kardos, H. Edskes, J. A. Carver, Y. Goto, A multi-pathway perspective on protein aggregation: implications for control of the rate and extent of amyloid formation. *FEBS Lett* **589**, 672-679 (2015).

45. B. M. Burmann *et al*., Regulation of alpha-synuclein by chaperones in mammalian cells. *Nature* **577**, 127-132 (2020).

46. R. Tira *et al*., Dynamic molecular exchange and conformational transitions of alpha-synuclein at the nano-bio interface. *Int J Biol Macromol* **154**, 206-216 (2020).

47. M. Ziaunys, T. Sneideris, V. Smirnovas, Self-inhibition of insulin amyloid-like aggregation. *Phys Chem Chem Phys* **20**, 27638-27645 (2018).

48. F. Hasecke *et al*., Origin of metastable oligomers and their effects on amyloid fibril self-assembly. *Chem Sci* **9**, 5937-5948 (2018).

49. L. Giehm, D. I. Svergun, D. E. Otzen, B. Vestergaard, Low-resolution structure of a vesicle disrupting α-synuclein oligomer that accumulates during fibrillation. *Proc Natl Acad Sci U S A* **108**, 3246-3251 (2011).

50. M. K. Janowska, K. P. Wu, J. Baum, Unveiling transient protein-protein interactions that modulate inhibition of alpha-synuclein aggregation by beta-synuclein, a pre-synaptic protein that co-localizes with alpha-synuclein. *Sci Rep* **5**, 15164 (2015).

51. J. K. Williams *et al*., Multi-Pronged Interactions Underlie Inhibition of alpha-Synuclein Aggregation by beta-Synuclein. *J Mol Biol* **430**, 2360-2371 (2018).

52. Y. K. Al-Hilaly *et al*., The involvement of dityrosine crosslinking in alpha-synuclein assembly and deposition in Lewy Bodies in Parkinson's disease. *Sci Rep* **6**, 39171 (2016).

53. A. Sanjeev, R. K. Sahu, V. S. K. Mattaparthi, Potential of mean force and molecular dynamics study on the transient interactions between alpha and beta synuclein that drive inhibition of alpha-synuclein aggregation. *J Biomol Struct Dyn* **35**, 3342-3353 (2017).

54. A. Peduzzo, S. Linse, A. K. Buell, The Properties of alpha-Synuclein Secondary Nuclei Are Dominated by the Solution Conditions Rather than the Seed Fibril Strain. *ACS Chem Neurosci* **11**, 909-918 (2020).

55. D. R. Boyer *et al*., The alpha-synuclein hereditary mutation E46K unlocks a more stable, pathogenic fibril structure. *Proc Natl Acad Sci U S A* **117**, 3592-3602 (2020).

56. X. Yang, J. K. Williams, R. Yan, M. M. Mouradian, J. Baum, Increased Dynamics of alpha-Synuclein Fibrils by beta-Synuclein Leads to Reduced Seeding and Cytotoxicity. *Sci Rep* **9**, 17579 (2019).

57. L. Kang *et al*., N-terminal acetylation of alpha-synuclein induces increased transient helical propensity and decreased aggregation rates in the intrinsically disordered monomer. *Protein Sci* **21**, 911-917 (2012).

58. O. Millet, J. P. Loria, C. D. Kroenke, M. Pons, A. G. Palmer, The static magnetic field dependence of chemical exchange linebroadening defines the NMR chemical shift time scale. *J Am Chem Soc* **122**, 2867-2877 (2000).

59. J. Schindelin *et al*., Fiji: an open-source platform for biological-image analysis. *Nat Methods* **9**, 676-682 (2012).

60. T. D. Schneider, R. M. Stephens, Sequence logos: a new way to display consensus sequences. *Nucleic Acids Res* **18**, 6097-6100 (1990).

61. G. E. Crooks, G. Hon, J. M. Chandonia, S. E. Brenner, WebLogo: a sequence logo generator. *Genome Res* **14**, 1188-1190 (2004).